

The method of forest change detection using Sentinel-2 optical satellite imagery and Sentinel-1 radar imagery: A case study in Dak Nong Province, Vietnam

TRAN QUANG BAO^{1,2,*}, NGUYEN VAN THI², LE SY DOANH², PHAM VAN DUAN², LA NGUYEN KHANG², NGUYEN TRONG CUONG², BUI TRUNG HIEU³, DAO THI THANH MAI², DINH VAN TUYEN¹

¹Vietnam Administration of Forestry. ²Ngoc Ha, Ha Noi, Vietnam. Tel./fax. +84-0945043274, *email: baofuv@vnuf.edu.vn

²Vietnam National University of Forestry. Xuan Mai Town, Ha Noi, Vietnam

³University of Adelaide, School of Agriculture. Food and Wine, Adelaide SA 5005, Australia

Manuscript received: 12 July 2022. Revision accepted: 13 September 2022.

Abstract. Bao TQ, Thi NV, Doanh LS, Duan PV, Khang LN, Cuong NT, Hieu BT, Mai DTT, Tuyen DV. 2022. The method of forest change detection using Sentinel-2 optical satellite imagery and Sentinel-1 radar imagery: A case study in Dak Nong Province, Vietnam. *Biodiversitas* 23: 4800-4809. This study presents the findings of forest change detection in Dak Nong Province, Vietnam by combining the NDVI of Sentinel-2 satellite imagery and the backscatter (BKS) values of VH and VV polarizations from the first quarter of 2020 to the first quarter of 2021 and using the combination model of BKS and NDVI (CMB) to determine the NDVI and Backscatter Change Index (NBCI) between the two periods, which were processed and analyzed in Google Earth Engine. The verification results on 270 samples for all 3 indices show that the results of forest loss detection using NBCI index, NDVI index, and BKS index reach 93.3%, 83.3% and 73.3%, respectively; the results of identifying the areas with no forest change using NBCI index, NDVI index, and BKS index achieve 97.8%, 92.2% and 83.3%, respectively; the results of forest increase detection using NBCI index, NDVI index, and BKS index reach 90.0%, 85.6% and 68.9%, respectively. The NBCI index for Dak Nong Province indicated that during the study period, the province lost 1,198.9 hectares forest area, whereas it gained 871.3 hectares of the same.

Keywords: BKS, Google Earth Engine, NBCI, NDVI, remote sensing

INTRODUCTION

Nowadays, the detection of changes in plant cover in general and forest cover in particular is frequently done using remote sensing and GIS technology. In addition, optical satellite imaging and ultra-high frequency data, commonly referred to as radar data, are two frequently used data types.

Due to the stability, consistency, and usability of the data, optical remote sensing, which was developed fairly early, offers a vast amount of information for assessing changes in land use. For instance, since 1972, Landsat images, since 1983, Landsat Thematic Mapper, since 1980, SPOT photos, since 1980, and since 1999, MODIS images have been widely utilised. The studies on a regional or national level often use satellite imagery with medium or high spatial resolution (for example, less than 100 m), such as Landsat or SPOT (Homer et al. 2007; Morton et al. 2011; Griffiths et al. 2014); however, with the advancement of computing and data processing capabilities, even global analysis can also be done using these data (Hansen et al. 2013). Global land-cover mapping programs often use data with a lower spatial resolution (≥ 250 m), such as “Medium Resolution Imaging Spectrometer (MERIS) for Global Cover” data (Bezy et al. 1997), “SPOT Vegetation for the Global Land Cover 2000” dataset (Bartholomé et al. 2005), “AVHRR for the University of Maryland Global Land Cover Classification

(Hansen et al. 2010), or “MODIS global land cover product” (Friedl et al. 2010). Nowadays, there are a lot of studies mentioning multi-temporal data analysis of optical data (Griffiths et al. 2012; Estel et al. 2015) or combined with spatially specific statistical data (Reddy et al. 2015), using a large volume of freely available optical data, especially those of Landsat (Hansen et al. 2013; Kovalsky and Roy 2013; Roy et al. 2014). The time series analysis allows to capture the entire change process compared with traditional multi-temporal image analysis (Hostert et al. 2015), as well as fill the gaps covered by clouds (Santos et al. 2019; Oehmcke et al. 2020).

The use of ultra-high frequency remote sensing technology for mapping land cover is not as common as optical remote sensing; it has only started to be employed in the last decade. Remarkably, the data from SAR systems such as “Spaceborne Imaging Radar – C/X-Band Synthetic Aperture Radar (SIR-C/X-SAR)”, “European Remote Sensing (ERS-1 and -2)”, “Advanced Synthetic Aperture Radar (ASAR)”, “Japanese Earth Resources Satellite (JERS-1)”, “RADARSAT-1 and -2”, “Advanced Land Observation Satellite (ALOS-1)”, etc., are commonly used and applied to the regional scale while very few studies address global-scale mapping (Shimada et al. 2014). On the other hand, there are a lot of studies on land-cover, including improvement of land-cover classification (Cable et al. 2014; Ryan et al. 2014), forest cover classification (Devaney et al. 2015; Ningthoujam et al. 2016), grassland

monitoring (Dusseux et al. 2014), assessment of forest degradation (Griffiths et al. 2012; Ryan et al. 2014), forest loss detection (Whittle et al. 2012), forest succession (Ryan et al. 2014). Similarly, specific studies on land use also focus on a variety of topics, such as urban land-use analysis (Wu et al. 2015; Stumpf et al. 2021), agricultural land use classification (Bargiel and Herrmann 2011), mapping and monitoring specific crops (Bouvet and Le 2011; Joshi et al. 2016; McNairn and Shang 2016).

Radar data is increasingly being used in combination with optical data to improve crop classification (Pereira et al. 2013; Joshi et al. 2016) and land management mapping (Stefanski et al. 2014; Ngo et al. 2020). Combining optical and radar satellite images in forest monitoring gives better results than using these data types separately (Thenkabail 2015; Hirschmugl et al. 2018). The classification result reaches up to 88% if using both ALOS/PALSAR and ALOS/AVNIR-2 while it is 77% if only using ALOS/AVNIR-2 (Hoan et al. 2012). If the data of Sentinel-1 and Sentinel-2 are combined, the classification result of land use and land cover in the Eastern Brazilian Amazon is up to 91.07%, while it is only 89.53% if only using Sentinel-2 data. Sentinel-1 data also needs to be applied more in forest surveys and monitoring in tropical zones (Tavares et al. 2019)

The advantages and drawbacks of optical and radar remote sensing, as well as the trend and potential for merging these two forms of data in land cover mapping and monitoring of land cover change, have all been demonstrated in both local and international research. To identify the regions of clear-cut forest throughout the province in the case study in Dak Nong, we used Sentinel-2 optical satellite images with Sentinel-1 radar satellite images. The study's findings will help improve the theoretical and practical foundations for using remote sensing technology to monitor changes in forest resources in Dak Nong Province and other regions with comparable conditions, enhancing the effectiveness of forest resource management and protection.

MATERIALS AND METHODS

Research materials

Sentinel-2 data (with a cloud coverage percentage of less than 30%) and Sentinel-1 data were utilised in this study. The data were separated into two periods, the first (K_t) covering the period from January 1 to March 31, 2020, and the second (K_s), covering the period from January 1 to March 31, 2021. The Sentinel-1 data was collected from Google Earth Engine (ee.ImageCollection('COPERNICUS/S1_GRD')) and processed to Level-1C with calibration and conversion of scattering value to decibels. This work combined the NDVI of Sentinel-2 images with descending and ascending data with VH and VV polarizations. Sentinel-2 data was also collected from Google Earth Engine (ee.ImageCollection('COPERNICUS/S2_SR')) and processed to Level-2A with atmospheric and geometric corrections.

Data processing method

Cloud removal in Sentinel-2 optical imagery

This study used cloud masking with multi-temporal images using offset method, where cloud-free areas in one image was used to replace cloudy areas in another image at the same location (Dial et al. 2003; Gómez-Chova et al. 2017) using the cloud detection algorithm integrated on the Google Earth Engine (GEE) based on the "QA60" band. After removing clouds, all bands of all images in the selected time series were merged using the *median()* function in the GEE to create a cloud-free image.

Sentinel-1 data processing

First, the combined data (AD) between the *Ascending* data and *Descending* data was created using the *merge()* function for each polarization: VH (vhAD) and VV (vvAD), then an average data (tbAD) was created between vhAD and vvAD with the formula: $tbAD = (vhAD + vvAD)/2$. Finally, the focal median value (comAD) of the 3 newly-created data was calculated using the *focal_median()* function: $comAD = ee.Image.cat([vhAD, vvAD, tbAD]).focal_median()$.

Calculating the indices

Normalized Difference Vegetation Index (NDVI) was calculated from 2 spectral bands, including NIR (near-infrared) and RED (red) according to the formula:

$$NDVI = \frac{NIR - RED}{NIR + RED} \quad (1)$$

Applying the formula (1) to calculate NDVI for K_t and K_s images will get $NDVI_t$ and $NDVI_s$. The NDVI of the Sentinel-2 satellite image is calculated in the GEE using the *normalizedDifference()* function with two bands, B8 and B4.

Sentinel-2's NDVI index and Sentinel-1's backscatter value (BKS) were combined together (CMB) through the formula:

$$CMB = (NDVI + \frac{-1}{BKS})/2 \quad (2)$$

The formula (3) is rewritten as follows:

$$CMB = \frac{NDVI * BKS - 1}{2 * BKS} \quad (3)$$

Because the BKS has a negative value, to be able to take the average value equivalent to NDVI, BKS is added a negative sign and inversed its value, that is, 1 divided by BKS, and adding a negative sign in front of the new value. When using this transformation, the new value will be covariate with the NDVI. The nature of formula (3) is the result of reducing fractions to a common denominator in order to make calculations more convenient in the GEE.

The formula (3) was applied to calculate CMB_t and CMB_s based on the NDVI and scattering value of the first period and second period.

NDVI and Backscatter Change Index (NBCI) is the percentage (%) between CMB_s and CMB_t , and was calculated using the following formula:

$$NBCI = \frac{CMB_s - CMB_t}{CMB_t} \times 100\% \tag{4}$$

Change threshold: When the NBCI is in the range around 0, which is known as the stable threshold (NV - No change Value), a forest is said to be stable. The NBCI below NV is known as the Reduce Value (RV), which corresponds to a reduction in forests, and the NBCI above NV is known as the Increase Value (IV), which corresponds to an increase in forests. The findings of experimental study using 90 samples were used to determine the values of NV, RV, and IV (30 actual samples with No change Value, 30 actual samples with Reduce Value, and 30 actual samples with Increase Value).

Identifying the areas of forest loss

After determining the change threshold, the NBCI images were reclassified according to the RV, NV and IV values. (i) The RV range was replaced with the value -1 (reduced change). (ii) The NV range was replaced with the value 0 (no change). (iii) The IV range was replaced with the value 1 (increased change).

The result of the reclassification is a raster containing the values 0 and 1. This raster was superimposed with the forest cover map of the first period to determine the areas of forest reduction. The changed areas on the reclassified raster that were outside the boundary of the 3 forest types or within the boundary of the 3 forest types but the status

quo was not forest was removed from the calculation results.

The whole research method is briefly described by the following diagram Figure 1.

RESULTS AND DISCUSSION

Cloud-masking results on Sentinel-2 satellite imagery

A series of photos with less than 30% cloud coverage underwent cloud masking in the GEE, resulting in the development of Sentinel-2 K_t and K_s images from 59 and 57 image sessions, respectively. The findings of the detection of forest change throughout the entire boundary of Dak Nong Province were unfalsified since the removal of the clouds had very little impact on the NDVI value.

To assess the possibility of using a set of images to create a cloud-free image in forest change detection, spectral value analysis for each band on the images of each observation period were conducted, whose results are presented in Table 1.

Table 1 shows that the statistical indicators of the bands' spectral values on the images after cloud masking in the first and second periods to be similar; especially, the spectral mean and the standard deviation between the respective bands of each observation period were the same. This result showed that it is appropriate to use composite images after cloud masking between two observation periods to compare the change in spectral values based on NDVI index (to combine with other factors) (Figure 2).

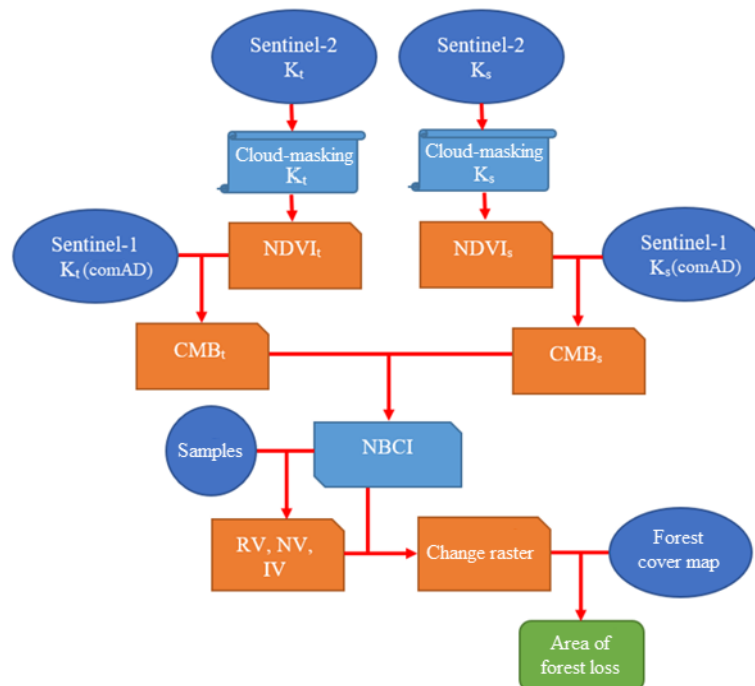


Figure 1. Process diagram for the study of forest change detection in Dak Nong Province, Vietnam using Sentinel-2 optical satellite imagery and Sentinel-1 radar imagery. CMB: Combination Model of Backscatter and NDVI; comAD: Combination of Sentinel-1 Ascending and Descending data; IV: Increase Value; NBCI: NDVI and BKS Change Index; NV: No change Value; RV: Reduce Value



Figure 2. A. Sentinel-2 image in the first period (after cloud masking), B. Sentinel-2 image in the second period (after cloud masking)

Table 1. Analysis of histogram values

Indicators	First period				Second period			
	Red	Green	Blue	NIR	Red	Green	Blue	NIR
Minimum	0.03	0.04	0.07	0.04	0.03	0.04	0.06	0.04
Maximum	0.43	0.36	0.33	0.42	0.54	0.46	0.46	0.45
Medium	0.07	0.09	0.10	0.11	0.07	0.09	0.09	0.14
Standard deviation	0.03	0.01	0.01	0.02	0.02	0.01	0.01	0.03

Calculation results of indices

The NDVI was calculated using the formula (1) for each single image after cloud removal, and then combined with each other using the *median()* function in the GEE in order to create NDVI raster for each observation period. Thus, $NDVI_t$ was generated from 59 component $NDVI_s$, and $NDVI_s$ were generated from 57 component $NDVI_i$.

Sentinel-1 scattering data of the first period was generated from 35 scans, and that of the second period was generated from 37 scans using the *median()* function in the GEE. The combined data between the NDVI and the scattering value were combined according to formula (3). The NDVI and Backscatter Change Index (NBCI) was calculated using formula (4).

Table 2 shows that the values of the indices in the first and second periods had a high similarity. This allows to compare the change in value between two observation periods at a certain location. Statistical analysis showed a significant difference among the NBCI, the BKS, NDVI and CMB. A very high standard deviation reflects large difference between values, which means that it is possible to distinguish forest increase and decrease by using the NBCI when a specific threshold is determined.

Determining the change threshold

The change threshold was determined on 90 actual samples for the NDVI, backscatter (BKS), and NDVI and Backscatter Change Index (NBCI), results of which are shown in Figure 7.

For NBCI the Reduce Values ranged from -129.42 to -34.78 and were mainly concentrated between -99.66 to -56.77; the No change Values ranged from -48.45 to 45.89 and were highly concentrated between -13.98 to 17.32; the Increase Values ranged from 40.30 to 92.99 and were mainly concentrated between 46.40 to 79.74. For NDVI the Reduce Values ranged from -85.18 to -27.60 and were mainly concentrated between -79.90 to -52.76; the No change Values ranged from -36.25 to 41.73 and were highly concentrated between -17.64 to 26.87; the Increase Values ranged from 29.80 to 89.27 and were mainly concentrated between 54.99 to 79.93. For BKS the Reduce Values ranged from 38.25 to 126.69 and were mainly concentrated between 81.27 to 98.18; the No change Values ranged from -49.16 to 47.78 and were highly concentrated between -23.26 to 24.79; the Increase Values ranged from -87.76 to -31.28 and were mainly concentrated between -69.96 to -48.86.

Table 2. statistically analyzes the indices to assess the change between two observation periods

Indicators	BKS		NDVI		CMB		NBCI
	BKS _t	BKS _s	NDVI _t	NDVI _s	CMB _t	CMB _s	
Minimum	-29.22	-29.05	-0.50	-0.51	-4.29	-4.30	-100,049.00
Maximum	7.77	8.17	0.84	0.85	2.11	2.12	1,062,818.00
Medium	-16.18	-15.95	0.52	0.53	0.29	0.30	5.78
Standard deviation	2.79	2.74	0.18	0.17	0.09	0.09	1,336.88

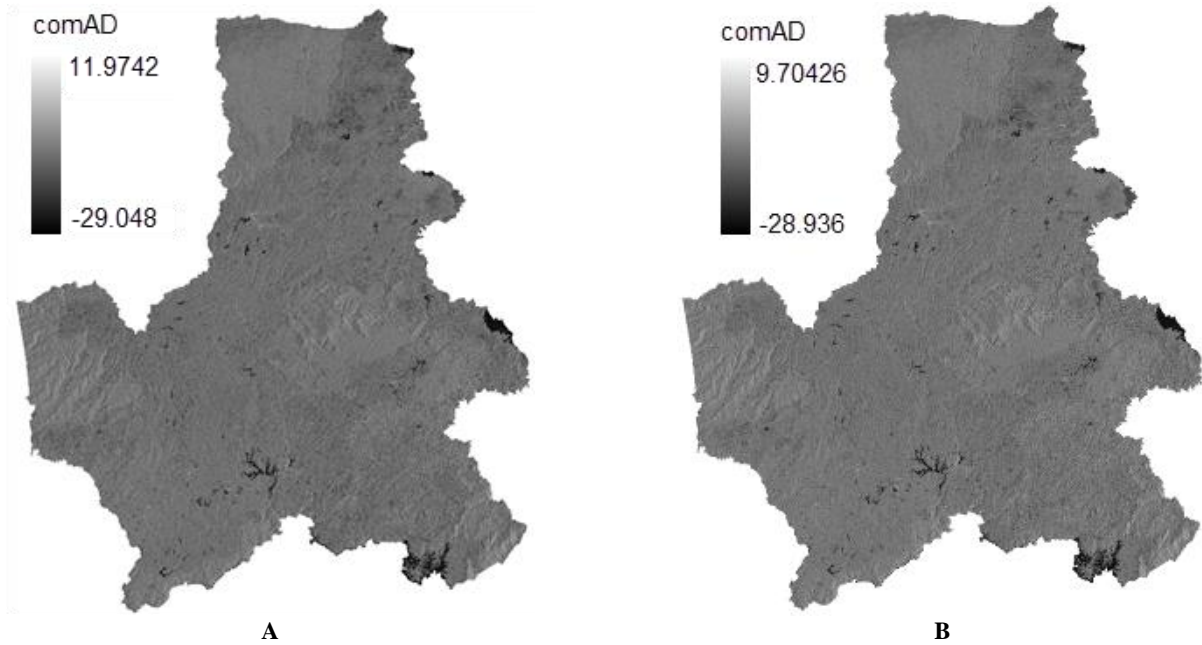


Figure 3. A. comAD in the first period (minimum: -29.048; maximum: 11.9742), B. comAD in the second period (minimum: -28.936; maximum: 9.70426)

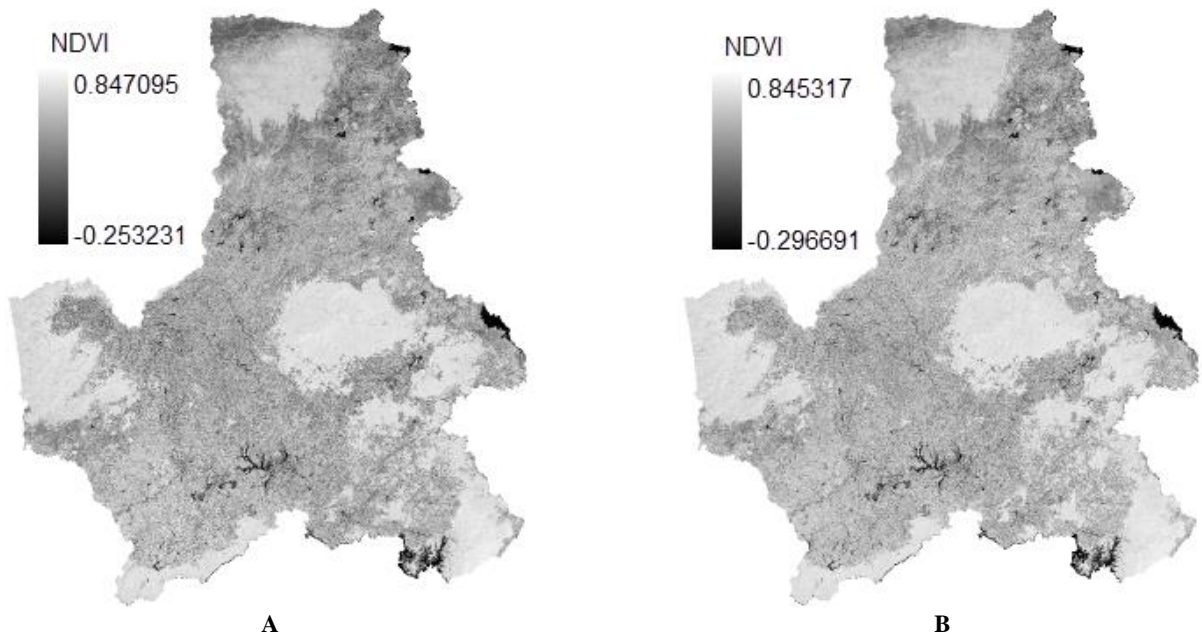


Figure 4. A. NDVI in the first period (minimum: -0.253231; maximum: 0.847095), B. NDVI in the second period (minimum: -0.296961; maximum: 0.845317)

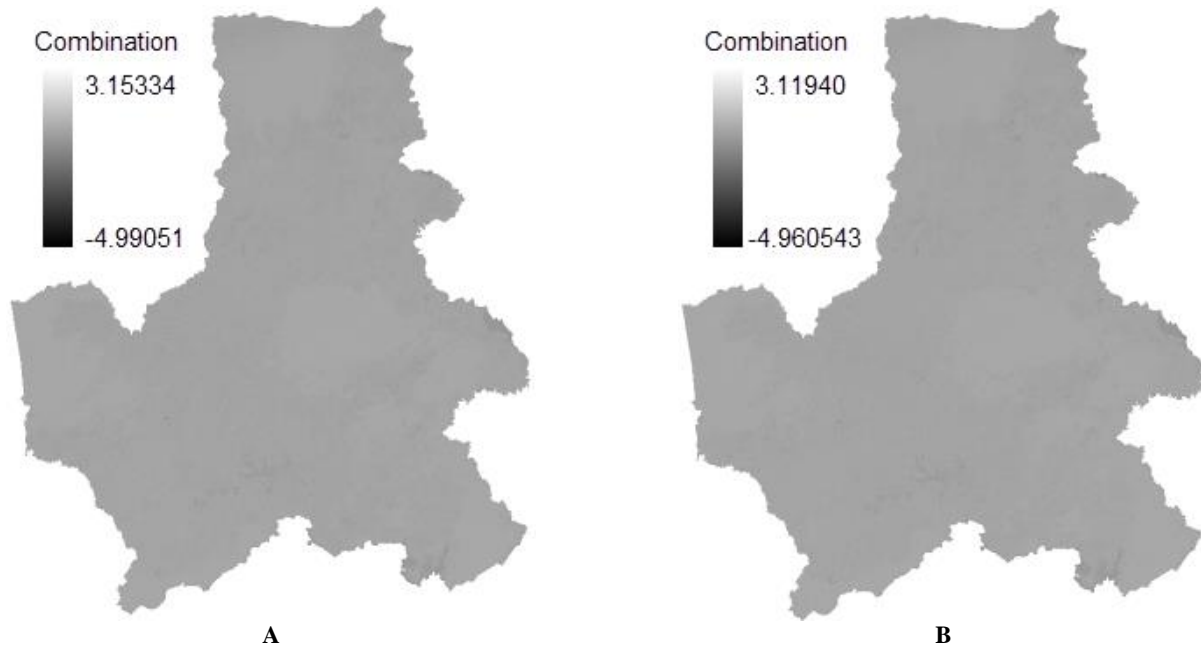


Figure 5. A. Combination in the first period (minimum: -4.99051; maximum: 3.15334), B. Combination in the second period (minimum: -4.960543; maximum: 3.1194)

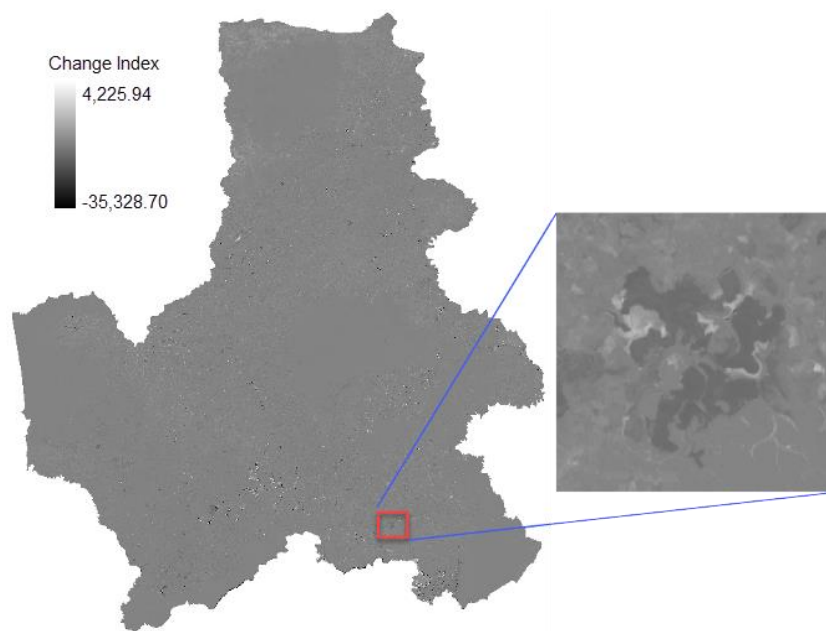


Figure 6. Change Index (minimum: -35328.7; maximum: 4225.94). The dark spots are the areas with high Reduce Value (RV), the bright spots are the areas with high Increase Value (IV), the rest are the stable areas (No change Value - NV)

Thus, the Increase Values, No change Values, and Reduce Values of the indices all have interference in a certain range; therefore, the forest increase/decrease threshold was determined as the median of the values in the interference range (Table 3, Figure 6).

The forest change detection threshold for each index is displayed in Table 3. For NBCI, it was observed that the forest area was stable between -40.89 and 44.56; values lower than -40.89 indicated a forest loss, while values

higher than 44.56 suggested an increase in the forest area. About NDVI, it was observed that the forest area was stable between -31.67 and 36.14; values lower than -31.67 indicated a loss of forest, while values higher than 36.14 showed an expansion of the forest. Finally, for BKS, it was found that the forest area was stable between -40.57 and 42.38; values lower than -40.57 indicated an increase in forest area, while values higher than 42.38 suggested a decrease in forest area.

Forest change detection

The classification threshold in Table 1 for each NBCI, NDVI, and BKS index was used to create forest change rasters. In these rasters, the pixels with values of -1 represent locations where the forest has been lost, 0 represent stable locations, and 1 represent locations where the forest has increased. To exclude pixels beyond the planning of the three forest types, these forest change rasters were integrated with the province of Dak Nong's forest cover map in 2021. The results from the NBCI index detected 4512 locations of forest loss, 12153 stable locations, 3544 locations of forest increase; the NDVI index detected 5031 locations of forest loss, 12655 stable locations, 4028 locations of forest increase; and the BKS index detected 6037 locations of forest loss, 12444 stable locations, and 4923 locations of forest increase.

Based on the results field verification were carried out with random sampling of 90 locations of forest loss, 90 stable locations, and 90 locations of forest increase to determine the percentage of correct detection (Table 4).

Table 4 shows that the NBCI have highest ability of forest change detection, and the BKS being the lowest. The ability of forest loss detection, the ability of forest stability detection, and the ability of forest increase detection by NBCI reached 93.3%, 97.8% and 90.0%, respectively.

The results of forest change statistics detected by the NBCI index showed that from the beginning of 2020 to the

beginning of 2021, the whole province lost 1,198.9 hectares of forest area, while the increase in areas of forest was 871.3 hectares, and 282,364.0 hectares had no change. Specific details are as show in Table 5.

Table 5 shows that the area of forest loss is mainly concentrated in Tuy Duc District (605.7 ha, accounting for 50.5% of the total area of forest loss in the province), of which: 557.7 ha of planted forest, 28.0 ha of natural forest. Gia Nghia town had the least area of forest loss, only 15.3 ha, including 14.8 ha of planted forests and 0.5 ha of natural forests. The remaining districts had the area of forest loss from 77.8 ha to 112.7 ha, mainly planted forest.

The highest increase in forest area was in Dak Song District with 325.0 ha (accounting for 37.3% of the total area of forest increase of the whole province), and Gia Nghia town had the least increase in forest area, only 4.6 ha (accounting for 0.5% of the total area of forest increase of the whole province). Forest area also increased in Tuy Duc, Dak Glong and Krong No Districts with the area of 226.2 ha, 123.1 ha and 107.8 ha, respectively (accounting for 26.0%, 14.1% and 12.4% change in forest cover). In the remaining districts, the forest area increased only about 11.4-60.4 ha. The increase in forest area was mainly attributed to the reforestation after the exploitation of production forests.

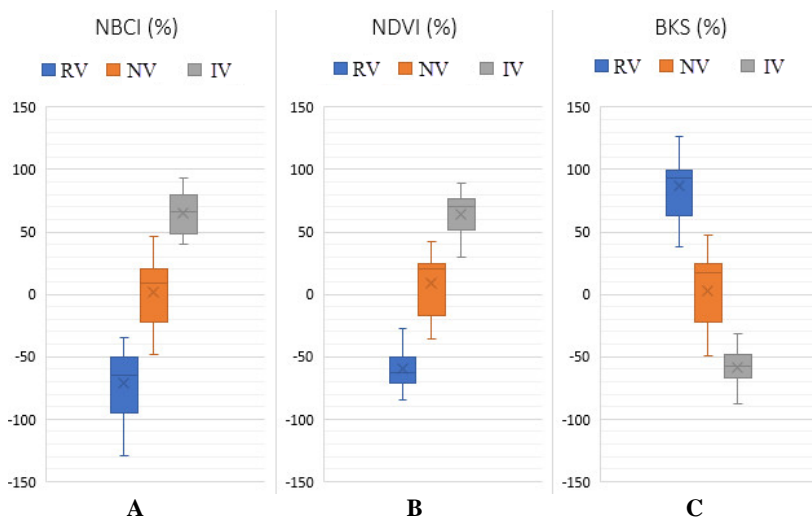


Figure 7. A. Change threshold for NBCI, B. Change threshold for NDVI, C. Change threshold for BKS

Table 3. Table showing forest change detection thresholds for NBCI, NDVI and BKS along with their interference range

Indices	Values in the interference range		Increasing/ reducing threshold	
	Reduce Value – No change Value	No change Value - Increase Value	Reduce Value	Increase Value
NBCI	-45.80; -42.63; -40.89; -40.39; -37.96; -35.33; -34.78; -48.45; -47.96; -45.04; -42.43; -38.71; -34.95	41.17; 44.84; 45.57; 45.89; 40.30; 41.74; 41.85; 44.56; 45.46	-40.89	44.56
NDVI	-32.46; -31.52; -30.58; -27.60; -36.25; -35.96; -33.96; -31.67; -30.44	35.77; 36.75; 36.76; 41.73; 29.80; 32.82; 34.24; 35.85; 36.43; 39.37	-31.67	36.14
BKS	38.25; 42.38; 46.28; 47.05; 33.78; 34.87; 37.70; 42.88; 47.78	-49.16; -45.94; -40.57; -38.32; -35.36; -48.86; -44.69; -41.72; -40.93; -39.15; -37.38; -35.72; -31.28	42.38	-40.57

Table 4. Field verification results

No.	Index	Change	Number of locations verified	Number of locations with correct detection	%
1	NBCI	Forest loss	90	84	93.3
		Forest stability	90	88	97.8
2	NDVI	Forest increase	90	81	90.0
		Forest loss	90	75	83.3
		Forest stability	90	83	92.2
3	BKS	Forest increase	90	77	85.6
		Forest loss	90	66	73.3
		Forest stability	90	75	83.3
		Forest increase	90	62	68.9

Table 5. Results of analysis of forest change using the NBCI index

No.	Districts	Total area	Forest loss	Forest stability	Forest increase
1	Cu Jut District	39,963.3	112.7	39,839.1	11.4
2	Dak Glong District	77,623.3	87.6	77,412.6	123.1
3	Dak Mil District	22,026.5	102.7	21,911.0	12.8
4	Dak R'Lap District	26,852.7	95.9	26,696.4	60.4
5	Dak Song District	26,960.7	77.8	26,557.8	325.0
6	Gia Nghia District	2,991.4	15.3	2,971.6	4.6
7	Krong No District	27,397.4	101.1	27,188.4	107.8
8	Tuy Duc District	60,619.0	605.7	59,787.1	226.2
	Total	284,434.2	1,198.9	282,364.0	871.3

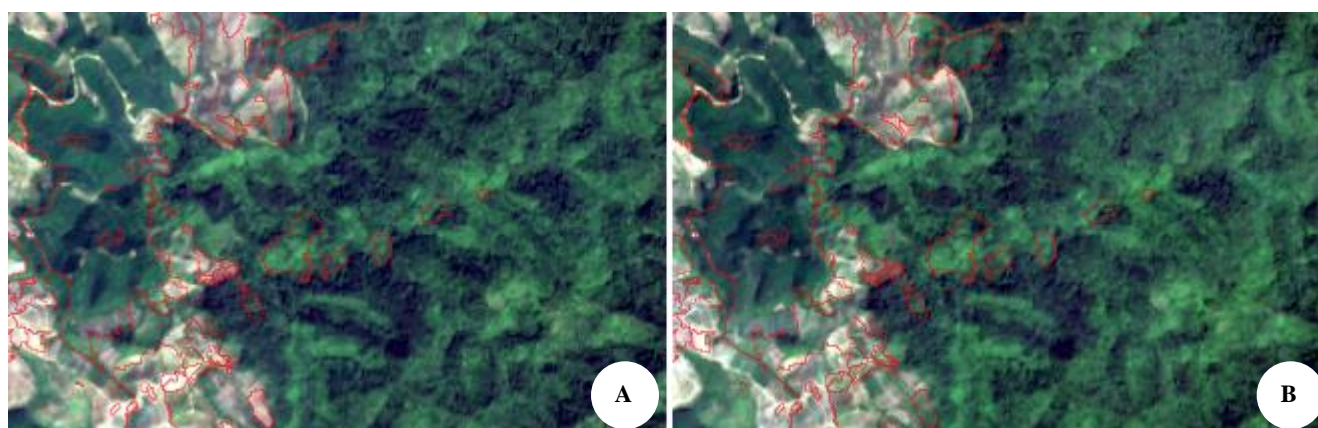
**Figure 8.** Satellite images before (A) and after (B) forest loss – Results detected by the NBCI index**Figure 9.** Satellite images before (A) and after (B) forest stability– Results detected by the NBCI index



Figure 10. Satellite images before (A) and after (B) forest increase – Results detected by the NBCI index

Discussion

When combining the backscatter value of Sentinel-1 satellite data with the NDVI index of Sentinel-2 satellite images, forest change detection in Dak Nong Province achieved higher accuracy than just using Sentinel-1 data or Sentinel-2 data. In this study, a combination of VH and VV polarizations was used in both *Descending* and *Ascending* dimensions of Sentinel-1 satellite data, which greatly increased the accuracy of forest change detection in Dak Nong Province. The use of multi-polarization with a two-dimensional scan has significantly reduced the influence of terrain (especially sloping terrain) and helped maximum observation of the surface in both directions. Radar data can analyze the surface structure of vegetation cover (Szigarski et al. 2018) and scattered forest areas more strongly than bare land areas. One limitation of this data is that it is difficult to detect whether the area is rich in vegetation or not; therefore, the combination with the NDVI index of the Sentinel-2 satellite imagery will support the analysis of changes in vegetation cover in general and forest cover in particular (Addabbo et al. 2016; Carrasco et al. 2019). The results of this study are also consistent with the study of (Tavares et al. 2019), which used both these types of data to classify the vegetation cover and achieved an accuracy of up to 91.07%.

In conclusion, the study uses Sentinel-2 optical satellite imagery and Sentinel-1 radar imagery to analyze the forest changes in Dak Nong Province in the first quarter of 2020-2021. The NBCI value was better than the NDVI and the BKS approach in forest change detection, in which forest loss detection reached 93.3%, forest gained detection was at 90%, and the detection of stability forest was at 97.8%. Following the NBCI index for Dak Nong Province, forest loss was 1,198.9 hectares of forest area, whereas forest gain was 871.3 hectares. The largest forest loss mainly occurred in the Tuy Duc District, around 50% of the total forest loss in Dak Nong Province. The largest forest increase was in Dak Son District, around 37% of the total area forest increase of the whole province. The NBCI index for Dak Nong Province indicated that during the study period, the province lost 1,198.9 hectares of forest area, whereas it gained 871.3 hectares of the same. For the change

threshold, the NBCI and BKS index had similar stable thresholds ranging from -40.89 to 44.56 and from -40.57 to 42.38, respectively. The NDVI index had a stable threshold ranging from -31.67 to 36.14. Because of cloud cover in the rainy season, using optical satellite images to detect forest loss in tropical areas in a short period is often difficult. Therefore, detecting deforestation requires a series of optical satellite images over a long enough time to filter clouds. Therefore, this result can be applied to assess forest cover changes over five years or more, giving more accurate results than annual or monthly monitoring.

ACKNOWLEDGMENTS

This research paper is the product of the National Science and Technology Project; Code: ĐTĐL.CN-01/20. On this occasion, the authors would like to express our deep gratitude to the Ministry of Science and Technology, Vietnam, for their interest in providing financial support for the research activities of the Project: “Study and propose solutions to stabilize agricultural production and people’s lives on forest land in the Central Highlands.”

REFERENCES

- Addabbo P, Focareta M, Marcuccio S, Votto C, Ullo SL. 2016. Contribution of Sentinel-2 data for applications in vegetation monitoring. *Acta Imeko* 5: 44-54. DOI: 10.21014/acta_imeko.v5i2.352.
- Bargiel D, Herrmann S. 2011. Multi-temporal land-cover classification of agricultural areas in two European regions with high resolution spotlight TerraSAR-X data. *Remote Sens* 3 (5): 859-877. DOI: 10.3390/rs3050859.
- Bartholomé E, Belward AS. 2005. GLC2000: A new approach to global land cover mapping from Earth observation data. *Int J Remote Sens* 26 (9): 1959-1977. DOI: 10.1080/01431160412331291297.
- Bezy JL, Delwart S, Gourmelon G, Bessudo R, Baudin G, Sontag H, Weiss S. 1997. Medium-resolution imaging spectrometer (MERIS). *Proc SPIE Advanced and Next-Generation Satellites II* 2957: 31-41. DOI: 10.1117/12.265446.
- Bouvet A, Le TT. 2011. Use of ENVISAT/ASAR wide-swath data for timely rice fields mapping in the Mekong River Delta. *Remote Sens Environ* 115 (4): 1090-1101. DOI: 10.1016/j.rse.2010.12.014.

- Cable JW, Kovacs JM, Shang J, Jiao X. 2014. Multi-temporal polarimetric RADARSAT-2 for land cover monitoring in Northeastern Ontario, Canada. *Remote Sens* 6 (3): 2372-2392. DOI: 10.3390/rs6032372.
- Carrasco L, O'Neil AW, Morton RD, Rowland CS. 2019. Evaluating combinations of temporally aggregated Sentinel-1, Sentinel-2 and Landsat 8 for land cover mapping with Google Earth Engine. *Remote Sens* 11 (3): 288. DOI: 10.3390/rs11030288.
- Devaney J, Barrett B, Barrett F, Redmond J, O'Halloran J. 2015. Forest cover estimation in Ireland using radar remote sensing: A comparative analysis of forest cover assessment methodologies. *PLoS One* 10 (8): e0133583. DOI: 10.1371/journal.pone.0133583.
- Dial G, Bowen H, Gerlach F, Grodecki J, Grodecki R. 2003. IKONOS satellite, imagery, and products. *Remote Sens Environ* 88 (1-2): 23-36. DOI: 10.1016/j.rse.2003.08.014.
- Dusseux P, Corpetti T, Hubert-Moy L, Corgne S. 2014. Combined use of multi-temporal optical and radar satellite images for grassland monitoring. *Remote Sens* 6 (7): 6163-6182. DOI: 10.3390/rs6076163.
- Estel S, Kuemmerle T, Alcántara C, Leversá C, Prishchepov A, Hostert P. 2015. Mapping farmland abandonment and recultivation across Europe using MODIS NDVI time series. *Remote Sens Environ* 163: 312-325. DOI: 10.1016/j.rse.2015.03.028.
- Friedl MA, Sulla-Menashe D, Tan B, Schneider A, Ramankutty N, Sibley A, Huang X. 2010. MODIS Collection 5 global land cover: Algorithm refinements and characterization of new datasets. *Remote Sens Environ* 114 (1): 168-182. DOI: 10.1016/j.rse.2009.08.016.
- Gómez-Chova L, Amorós-López J, Mateo-García G, Muñoz-Marí J, Camps-Valls G. 2017. Cloud masking and removal in remote sensing image time series. *J Appl Remote Sens* 11 (1): 015005. DOI: 10.1117/1.JRS.11.015005.
- Griffiths P, Kuemmerle T, Baumann M, et al. 2014. Forest disturbances, forest recovery, and changes in forest types across the Carpathian ecoregion from 1985 to 2010 based on Landsat image composites. *Remote Sens Environ* 151: 72-88. DOI: 10.1016/j.rse.2013.04.022.
- Griffiths P, Kuemmerle T, Kennedy RE, Abrudan IV, Knorn J, Hostert P. 2012. Using annual time-series of Landsat images to assess the effects of forest restitution in post-socialist Romania. *Remote Sens Environ* 118: 199-214. DOI: 10.1016/j.rse.2011.11.006.
- Hansen MC, Defries RS, Townshend JRG, Sohlberg R. 2010. Global land cover classification at 1 km spatial resolution using a classification tree approach. *Intl J Remote Sens* 21 (6-7): 1331-1364. DOI: 10.1080/014311600210209.
- Hansen MC, Potapov PV, Moore R et al. 2013. High-resolution global maps of 21st-century forest cover change. *Science* 342 (6160): 850-853. DOI: 10.1126/science.1244693.
- Hirschmugl M, Sobe C, Deutscher J, Schardt M. 2018. Combined use of optical and synthetic aperture radar data for REDD+ applications in Malawi. *Land* 7 (4): 116. DOI: 10.3390/land7040116.
- Hoan NT, Tateishi R, Alsaaidh B, Ngigi T, Alimuddin I, Johnson B. 2012. Tropical forest mapping using a combination of optical and microwave data of ALOS. *Intl J Remote Sens* 34 (1): 139-153. DOI: 10.1080/01431161.2012.709329.
- Homer CG, Dewitz J, Fry J et al. 2007. Completion of the 2001 national land cover database for the conterminous United States. *Photogramm Eng Remote Sens* 73 (4): 337-341.
- Hostert P, Griffiths P, van der Linden S, Pflugmacher D. 2015. Time series analyses in a new era of optical satellite data. In: Kuenzer C, Dech S, Wagner W (eds). *Remote Sensing Time Series*, vol 22, Springer, Cham. DOI: 10.1007/978-3-319-15967-6_2.
- Joshi N, Baumann M, Ehammer A et al. 2016. A review of the application of optical and radar remote sensing data fusion to land use mapping and monitoring. *Remote Sens* 8 (1): 70. DOI: 10.3390/rs8010070.
- Kovalskyy V, Roy DP. 2013. The global availability of Landsat 5 TM and Landsat 7 ETM+ land surface observations and implications for global 30m Landsat data product generation. *Remote Sens Environ* 130: 280-293. DOI: 10.1016/j.rse.2012.12.003.
- McNairn H, Shang J. 2016. A review of multitemporal synthetic aperture radar (SAR) for crop monitoring. In: Ban Y (eds). *Multitemporal Remote Sensing*. Remote Sensing and Digital Image Processing, vol 20. Springer, Cham. 317-340. DOI: 10.1007/978-3-319-47037-5_15.
- Morton D, Rowland C, Wood C et al. 2011. Final report for LCM2007-the new UK land cover map. Countryside survey technical report no 11/07. Centre for Ecology & Hydrology (Natural Environment Research Council). Retrieved from <https://www.ceh.ac.uk/sites/default/files/LCM2007%20Final%20Report.pdf>, accessed on 08.02.2022
- Ngo KD, Lechner AM, Vu TT. 2020. Land cover mapping of the Mekong Delta to support natural resource management with multi-temporal Sentinel-1A synthetic aperture radar imagery. *Remote Sens Appl Soc Environ* 17: 100272. DOI: 10.1016/j.rsase.2019.100272.
- Ningthoujam RK, Tansey K, Baltzer H et al. 2016. Mapping forest cover and forest cover change with airborne S-Band Radar. *Remote Sens* 8 (7): 577. DOI: 10.3390/rs8070577.
- Oehmcke S, Chen THK, Prishchepov AV, Gieseke F. 2020. Creating cloud-free satellite imagery from image time series with deep learning. *Proceedings of the 9th ACM SIGSPATIAL International Workshop on Analytics for Big Geospatial Data* 1-10. DOI: 10.1145/3423336.3429345.
- Pereira LDO, Freitas CDC, Sant'Anna SJS et al. 2013. Optical and radar data integration for land use and land cover mapping in the Brazilian Amazon. *GIScience Remote Sens* 50 (3): 301-321. DOI: 10.1080/15481603.2013.805589.
- Reddy CS, Jha CS, Diwakar PG, Dadhwal VK. 2015. Nationwide classification of forest types of India using remote sensing and GIS. *Environ Monit Assess* 187 (12): 777. DOI: 10.1007/s10661-015-4990-8.
- Roy DP, Vulder MA, Loveland TR et al. 2014. Landsat-8: Science and product vision for terrestrial global change research. *Remote Sens Environ* 145: 154-172. DOI: 10.1016/j.rse.2014.02.001.
- Ryan CM, Berry NJ, Joshi N. 2014. Quantifying the causes of deforestation and degradation and creating transparent REDD+ baselines: A method and case study from central Mozambique. *Appl Geogr* 53: 45-54. DOI: 10.1016/j.apgeog.2014.05.014.
- Santos CLMdO, Camargo Lamparelli RA, Araújo Figueiredo GKD et al. 2019. Classification of crops, pastures, and tree plantations along the season with multi-sensor image time series in a subtropical agricultural region. *Remote Sens* 11 (3): 334. DOI: 10.3390/rs11030334.
- Shimada M, Itoh T, Motooka T et al. 2014. New global forest/non-forest maps from ALOS PALSAR data (2007-2010). *Remote Sens Environ* 155: 13-31. DOI: 10.1016/j.rse.2014.04.014.
- Stefanski J, Kuemmerle T, Chaskovskyy O et al. 2014. Mapping land management regimes in western Ukraine using Optical and SAR data. *Remote Sens* 6 (6): 5279-5305. DOI: 10.3390/rs6065279.
- Stumpf T, Bigman DP, Day DJ. 2021. Mapping complex land use histories and urban renewal using ground penetrating radar: A case study from Fort Stanwix. *Remote Sens* 13 (13): 2478. DOI: 10.3390/rs13132478.
- Szigarski C, Jagdhuber T, Baur M et al. 2018. Analysis of the radar vegetation index and potential improvements. *Remote Sens* 10 (11): 1776. DOI: 10.3390/rs10111776.
- Tavares PA, Beltrão NE, Guimarães US, Teodoro AC. 2019. Integration of Sentinel-1 and Sentinel-2 for Classification and LULC Mapping in the Urban Area of Belém, Eastern Brazilian Amazon. *Sensors* 19 (5): 1140. DOI: 10.3390/s19051140.
- Thenkabail PS. 2015. *Land Resources Monitoring, Modeling, and Mapping with Remote Sensing*. CRC Press Inc., Florida. DOI: 10.1201/b19322.
- Whittle M, Quegan S, Uryu Y et al. 2012. Detection of tropical deforestation using ALOS-PALSAR: A Sumatran case study. *Remote Sens Environ* 124: 83-98. DOI: 10.1016/j.rse.2012.04.027.
- Wu W, Guo H, Li X et al. 2015. Urban land use information extraction using the ultrahigh-resolution Chinese airborne SAR imagery. *IEEE Trans Geosci Remote Sens* 53 (10): 5583-5599. DOI: 10.1109/TGRS.2015.2425658.